Academic Journal of Science and Technology
ISSN: 2771-3032 | Vol. 18, No. 3, 2025

Thermal Deformation Analysis of Bionic Bee Wing Groove Dry Gas Seal

Ling Zeng, Wenjie Xi, Heshun Wang *, Weibing Zhu

University of Mechanical Enginering, Xihua University, Chengdu, Sichuan 610039, China

* **Corresponding author:** Heshun Wang (Email: wangheshun@mail.xhu.edu.cn)

Abstract: In order to solve the problems of insufficient opening force and insufficient stability of end face lubrication under the condition of frequent start and stop of dry gas seal or medium and low speed, a bionic bee wing groove dry air seal was designed and studied. Different from the traditional spiral groove, the WIHS bee wing structure is divided into main wings and auxiliary wings, forming a double-wide channel inlet design, through the double-wide channel inlet and narrow groove root, it can form a more stable air film during operation. The finite element method was used to analyze the thermal deformation and force deformation of the WIHS model imitation bee wing trough texture of silicon carbide material, and the waviness and taper deformation of the sealing end face were studied, and the following key conclusions were drawn: under the influence of thermal deformation, the waviness deformation of the WIHS model showed a three-period approximate chord function transformation law, and the taper deformation showed a trend of first decreasing and then increasing, and there were different degrees of taper deformation in the inner and outer diameters of the moving ring, and the taper deformation of the outer diameter was greater. Under the influence of force deformation, the amplitude of the waviness deformation is relatively stable, but the total deformation is larger, and the taper deformation increases first and then decreases from the inner diameter to the outer diameter.

Keywords: Bionic Honeybee Wing-shaped Grooves; Waviness Distortion; Taper Deformation; Thermal Deformation; Force Deformation.

1. Introduction

Designing and optimizing dry gas seal structures with excellent sealing performance and dynamic characteristics has always been a core research focus and a hot topic in the field of rotating machinery. This is not only a key approach to improving the vibration performance[1-2] and operational stability of high-speed rotating machinery, but also essential for addressing practical problems in this field.

Previous studies [3-4] have shown that by gaining a deeper understanding of the structure and function of organisms, and attempting to imitate their characteristics for application in end-face groove textures, optimizing groove parameters or modifying designs can achieve better sealing performance. For example, Wang Yanhong [5] used a bionic design inspired by bat wings to study the effects of high-speed stability, frictional thermal deformation, and transient working conditions on sealing performance. Jiang Jinbo [6], based on the wing structure of birds, conducted a bionic design of dry gas seal end-face grooves, analyzing geometric correlations through statistical methods, performing numerical simulations and experimental verification, and proposed high-performance bionic grooves (clustered bionic grooves and micro-row bionic grooves).

By discussing the living habits and working methods of bees from the perspective of their external structure, it was found that the movement of bee wings satisfies aerodynamics [7] and has a certain correlation with the formation of dry gas-sealed air films. This paper uses the shape of bee wings to construct the texture of the sealing end surface and designs a WIHS [8] bionic bee-wing-shaped groove dry gas seal. The finite element method is used to perform thermal and mechanical deformation analysis of the WIHS model with bee-wing groove texture made of silicon carbide material. By studying the variation patterns of the sealing end surface waviness and taper deformation, and comparing the analysis results of the waviness deformation and taper deformation of the sealing end surface, more accurate stress and deformation distribution patterns are obtained.

2. Hot Flow Deformation Analysis Model

2.1. Structural Parameters and Working Condition Parameters

The WIHS model's external structure features a larger main wing and a smaller secondary wing, with a wider wingtip structure serving as the fluid inlet for pumping fluid, as shown in Figure 1. The bionic groove model, end-face geometric parameters, and sealing condition parameters are shown in Figure 1, Table 1, and Table 2.

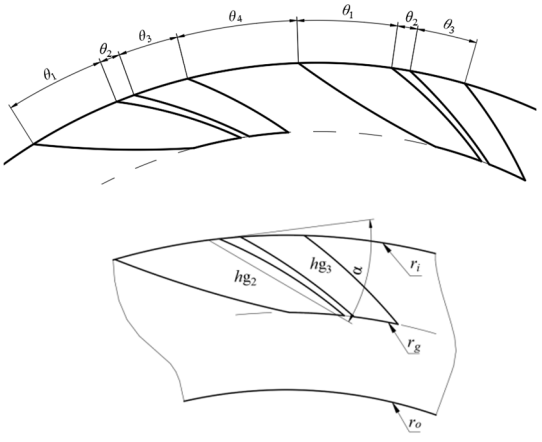


Figure 1. WIHS structural parameters

Table 1. Geometrical Parameters of the Bio-inspired Groove End Face

Parameter	WIHS
End face outer diameter (r_o/mm)	93
End Face Inner Diameter (r_i/mm)	70
Groove Root Radius (r_g /mm)	81.5
Groove Depth (h_{g2}/h_{g3}/μm)	8/6
Number of slots (n)	12
End face clearance (h_0/μm)	2
Biomimetic groove area (S/mm2)	268

Table 2. Sealing Operating Parameters

Parameter	Numerical value
Rotational Speed (n/rpm)	10000
Pressure Inlet (p_o/Mpa)	10
Pressure Outlet (p_i/Mpa)	0.1
medium	N_2

2.2. Hot Deformation Solution Model

2.2.1. Thermal Fluid-Solid Coupling Calculation Model

The friction end surface fluid-solid coupling calculation model is shown in Figure 2, including: a moving ring, a static ring, and a wedge-shaped liquid film formed between the moving and static rings



Figure 2. Thermal-fluid-structure interaction calculation model

2.2.2. Meshing and Irrelevance Verification

When performing force deformation analysis on the solid domain, the static ring is compensated by the elastic support due to its deformation, so no detailed analysis is performed here. Therefore, the pressure deformation mainly occurs in the moving ring. The mesh division of the end face of the moving ring is shown in Figure 3.



Figure 3. WIHS Solid domain mesh model

The total deformation is selected as the main object to verify the mesh independence, as shown in Figure 4. After calculation and verification, the calculation error does not exceed 1% after the grid unit is about 11,000. Therefore, the grid unit of about 11,000 is used to study the deformation and stress issues of the dynamic and static rings.

2.3. Dynamic Ring Model Thermal Boundary Settings

The boundary conditions of the moving ring model mainly consist of two boundary conditions, as shown in Figure 5. The moving ring boundary *no* is a general boundary with fixed support, and the remaining boundaries are in contact with the liquid film or air and are set as thermal boundary conditions.

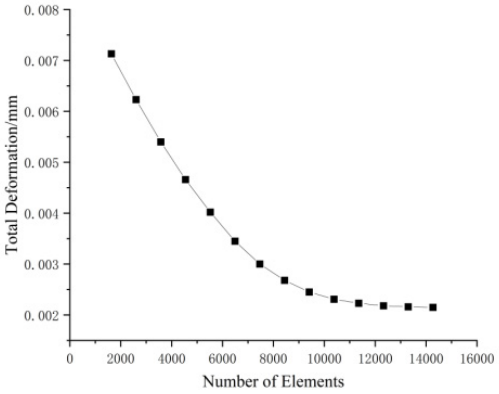


Figure 4. Validation of mesh-independence in the solid domain



Figure 5. Boundary model of the moving ring

Here, the thermal boundary conditions of the moving ring are assumed as shown in Table 3:

Table 3. Thermal boundary

Thermal boundary conditions	Boundary name
Viscous shear heat generated by the air film on the end face of the dynamic and static rings Q_V	*pq*
Forced convection heat transfer coefficient between the moving ring end surface and the air h_w	*pq*
Natural convection heat transfer coefficient between moving ring and air h_A	*Qr, rk, kl, lm, mn, op*

Under normal operating conditions of a dry gas seal, the main heat source is the gas viscous friction heat generated by the seal end face. The calculation formula of viscous friction heat [9]is:

$$Q_V = q_v A_f \tag{1}$$

In the formula, qv is the heat flow density; μ is the gas dynamic viscosity, Pa·s; r is the outer diameter of the sealing

end face; m is the sealing operating angular velocity, rad/s;h is the air film thickness, m;A_f is the sealing end facearea,m^2.

According to the fluid physical properties and flow form, different formulas are used to calculate the convection heat transfer coefficient for different convection heat transfer boundaries. Among them, the convection heat transfer h of the moving ring is the same as that of the horizontal rotating cylinder, and the formula is [10]:

$$Nu_D = 0.107\,\mathrm{Re}_D^{2/3}\,\mathrm{Pr}^{1/3} \tag{2}$$

$$h = \frac{Nu_D k}{D} \tag{3}$$

The end surfaces of the dynamic and static rings are considered to be high-speed fluid channels, so they are similar to forced convection on flat plates [11] The calculation formula is:

$$Nu = 0.664 \cdot \mathrm{Re}_L^{1/2} \cdot \mathrm{Pr}^{1/3} \tag{4}$$

In the formula, Pr is the Planck number, $\mathrm{Pr} = \frac{c_p \mu}{k}$; Re_D and Re_L both are the Reynolds number, U is the characteristic flow velocity of the gas, m/s; p is the gas density, D is the diameter of the rotating surface, m;L is the characteristic length, m; is the dynamic viscosity of the gas, Pa·s; c_p is the specific heat capacity at constant pressure, J/(kg·K); k is the thermal conductivity, W/(m·K).

The calculated thermal boundary values and selected sealing ring material parameters based on the derivation are shown in Table 4 and Table 5

Table 4. Thermal boundary calculation value

Thermal boundary	Numerical value
pq	q_v=121556.3 W/m2
pq	h_w=359.8(m²·K)
Qr, rk, kl, lm, mn	h_{A0}= 173. 8W/(m²·K)
op	h_{Ai}=158 W/(m²·K)

Table 5. Seal ring material parameters

Property	SIC
Density kg/m³	3100
Thermal expansion coefficient K⁻¹	3e-6
Young's modulus GPa	400
Poisson's ratio	0.17

3. Result Analysis

The deformation of the sealing end face is often reflected by circumferential unevenness and radial plane deviation. Circumferential flatness measurement usually involves the height deviation between the measured surface and the ideal plane. By selecting and relative to an ideal straight line a that passes through the axis of the torus, the unevenness of the torus in the radial direction (is, radial plane deviation [12]) can be obtained. By selecting the circular trajectory b that is concentric with the torus, the unevenness of the torus in the circumferential direction (is, circumferential unevenness[13-14]) can be obtained. The solid domain mesh model is shown in Figure 6.

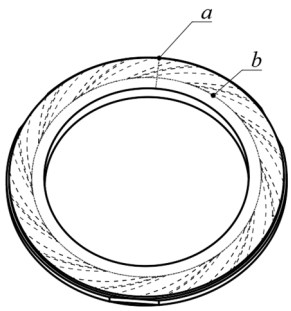


Figure 6. Solid domain mesh model

3.1. Thermal Deformation Analysis

As shown in Figure 7, a large amount of heat on the end surface of the WIHS model is concentrated at the contact friction surface and local heat is concentrated in the dam area and weir area of the moving ring. The temperature in the groove area is lower than the temperature in the dam area and weir area. The main reason for this is that friction heat is generated in the dam area and groove area due to the friction between the dynamic and stationary ring end faces when the air film is not formed, but the groove area does not participate in friction, resulting in a higher temperature in the former.

The study of the cutting dam area found that the temperature increases from the outer diameter to the inner diameter. The main reason is that when the gas flows from the high-pressure area of the outer diameter to the low-pressure area of the inner diameter, the rotation of the end face causes the gas molecules to violently collide in the gap channel to generate viscous heat, and the convection heat transfer of the outer diameter is more intense than that of the inner diameter, exacerbating the rising trend of temperature from the outside to the inside.

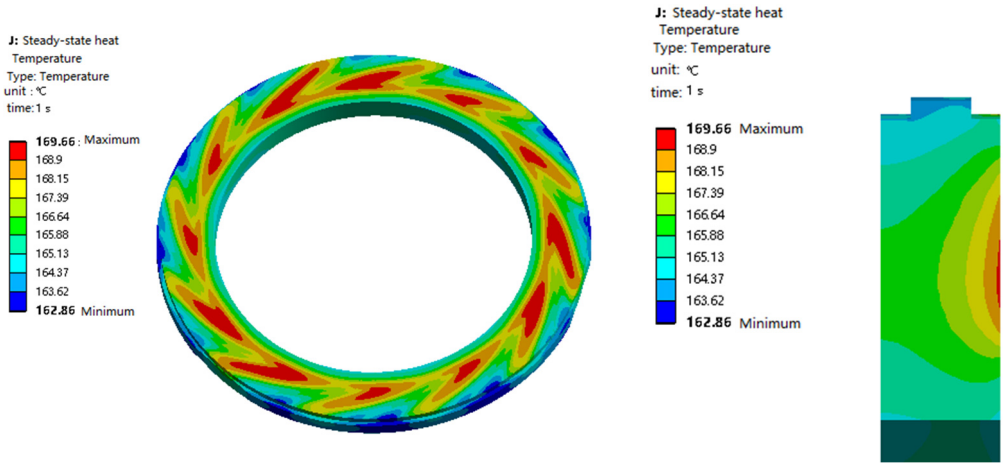


Figure 7. WIHS temperature field distribution contour map

Using the circular trajectory b (r_1=74.5mm), the circumferential unevenness of the moving ring annulus under thermal deformation is obtained. As shown in Figure 8, the maximum deviation from peak to peak trough of the WIHS model of silicon carbide material is $2.75\times10^{-6,}$ and the waviness deformation presents a three-period approximation to the chord function transformation law.

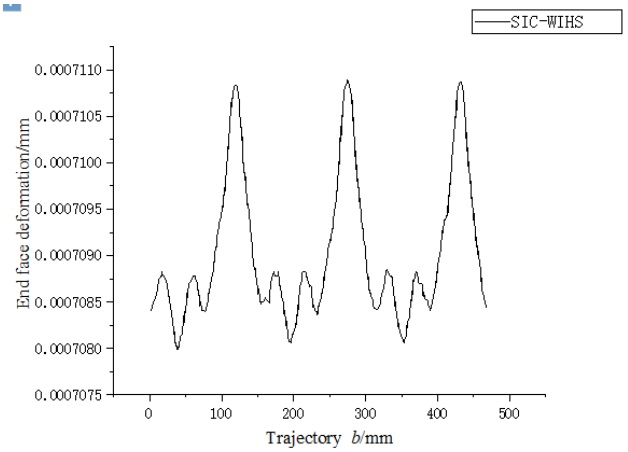


Figure 8. Radial unevenness distribution caused by temperatures at r_1 = 74.5mm

As shown in Figure 9, the end face taper deformation shows a trend of first decreasing and then increasing. The inner taper of the silicon carbide moving ring is 7.5×10^{-4}, and the outer taper is 2×10^{-3}, indicating that there are different taper deformations in the inner and outer diameters of the moving ring, and the outer diameter has greater taper deformation.

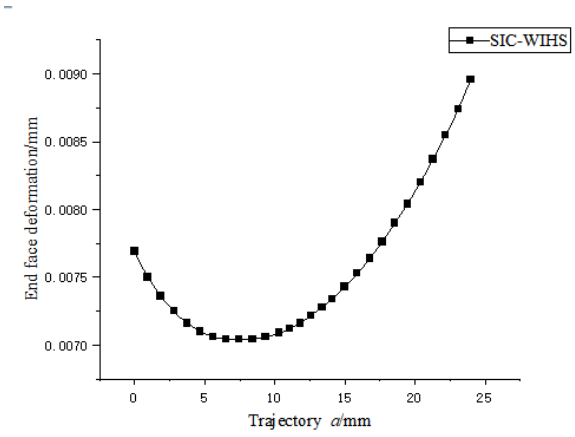


Figure 9. Radial plane deviation caused by temperatures at r_1= 74.5 mm

3.2. Force Deformation Analysis

Introducing the axial force of the air film into the static structure can obtain the end face deformation of the dynamic ring caused by the pressure of the air film flow field, as shown in Figure 10. The air film pressure is evenly distributed and produces large pressure deformation in the groove area; this is due to the hydrodynamic pressure effect, where pressure converges at the groove root to create a high-pressure area.

The study of the cutting dam area found that the pressure deformation gradually decreases from the outer diameter to the inner diameter. High-pressure gas flows in from the outer diameter side of the seal and generates a dynamic pressure effect through the groove structure. The "pumping effect" of the groove area pumps the gas into the sealing surface to form a high-pressure gas film with the highest pressure peak. Inner diameter direction: The gas flows toward the inner diameter after leaving the groove area. Due to the lack of groove dynamic pressure support, and the gap may gradually increase in the form of divergent flow channels, resulting in rapid pressure attenuation.

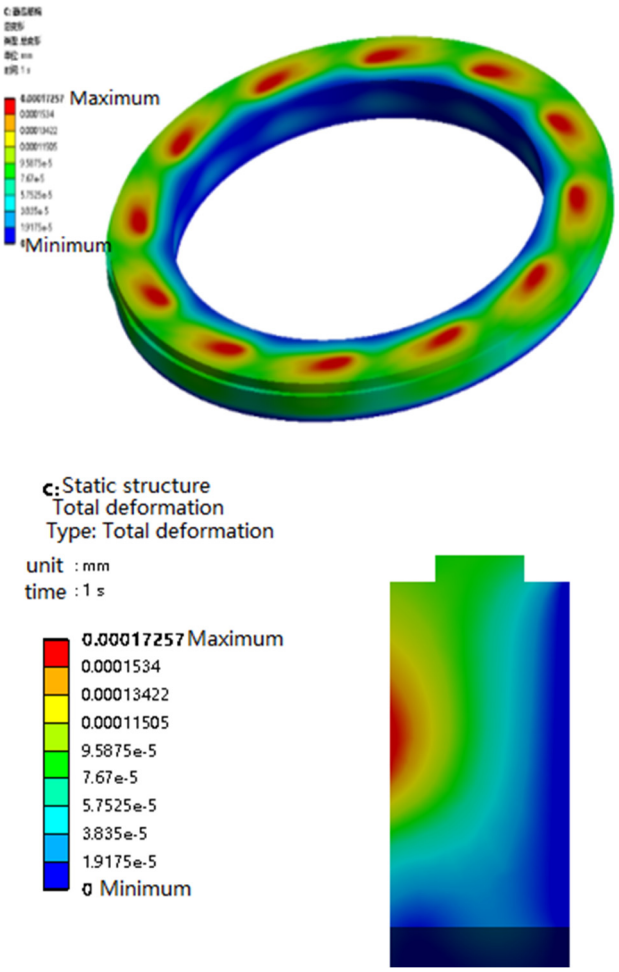


Figure 10. WIHS Pressure field deformation illustration

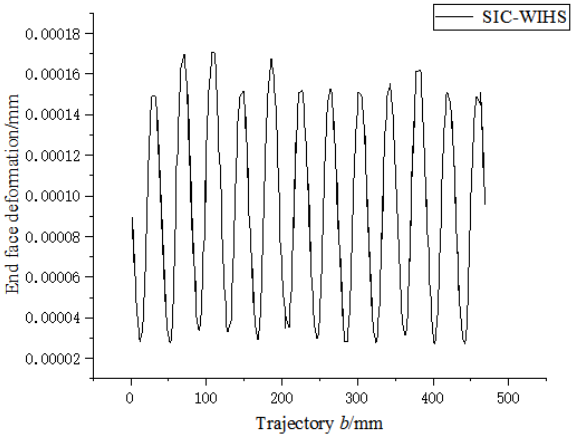


Figure 11. Radial unevenness distribution caused by pressure in the flow field at r1 = 74.5 mm

As shown in Figure 11, the WIHS model detects a large waviness deformation value at the circular trajectory b (r_1 = 74.5mm), indicating that pressure convergence occurs at the

groove root, causing the waviness to become larger. From the image, the waviness amplitude of the WIHS model is relatively stable, but the total deformation is large. This shows that the WIHS model is less affected by the geometric gap structure of the moving ring.

As shown in Figure 12, the taper change pattern of the WIHS dynamic ring overall model shows a distribution pattern that first increases and then decreases from the inner diameter to the outer diameter.

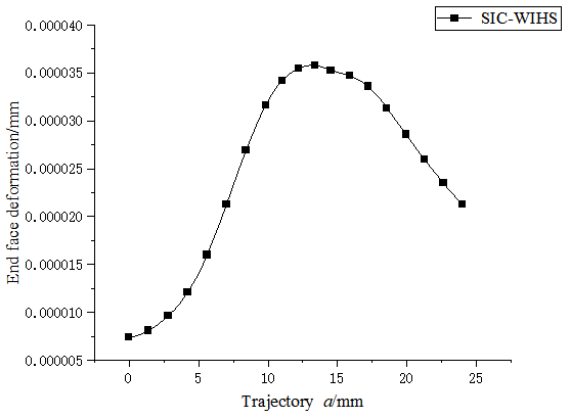


Figure 12. Radial plane deviation caused by temperatures

4. Conclusion

Through the above simulation calculation analysis, the following conclusions can be drawn:

(1) The WIHS bee wing structure consists of a main wing and an auxiliary wing. It adopts a double-wide channel inlet design, in which the air film fluid inlet is wider. This design allows it to have better anti-disturbance characteristics of the air film during high-speed rotation. At the same time, the double-wide channel entrance formed by the main and auxiliary fins and the narrow groove root can form a more stable air film when the equipment is running.

(2) Under the influence of thermal deformation, due to the uneven distribution of temperature and the gap problem in the moving ring structure, the thermal deformation fluctuations of the end surface also show a three-period approximate chord function transformation law. When the detection line b is closer to the outer diameter of the moving ring, the end surface waviness deformation becomes larger and the amplitude change becomes more stable. This is mainly due to the small periodic amplitude fluctuation of the inner diameter and the thermal structure of the outer diameter notch acting differently at different positions. The taper deformation first decreases and then increases. This is because the temperature is concentrated in the inner area of the annulus, resulting in a large temperature difference between the inner side of the annulus and the outer and inner diameters, which in turn leads to significant changes in the relative deformation at the outer and inner diameters. Moreover, there are varying degrees of taper deformation in the inner and outer diameters of the moving ring, and the taper deformation in the outer diameter is greater.

(3) Under the influence of force deformation, the WIHS model detects a large waviness deformation value in the circular trajectory b (r_1=74.5mm), indicating that pressure convergence occurs at the groove root, resulting in larger waviness. The waviness amplitude is relatively stable, but the total deformation is large. This shows that the WIHS model is less affected by the geometric gap structure of the moving ring. The taper change pattern of the model shows a distribution pattern that first increases and then decreases from the inner diameter to the outer diameter.

References

[1] LIU Wei, ZHANG Shuyao, ZHAI Zhixing, et al. Classification method of friction and vibration signal of floating ring seal based on QSE-ResNet [J]. Vibration and Shock, 2024, 43(21):194-201.) DOI:10. 13465/j. cnki.jvs. 2024.21.022.

[2] JIN Saisai, SUN Jianjun, MA Chenbo.Research on axial vibration of non-contact mechanical seal based on Newmark-β method[J].Lubrication and Sealing, 2024, 49(07):23-30.

[3] Cui Bowen, Ding Xuexing, Wang Shipeng, et al.Research on the performance analysis and design of dry gas seal of bionic carp tail groove[C]//Industry-University-Research Working Committee of Chinese Mechanics Society. Proceedings of the 20th China CAE Engineering Analysis Technology Annual Conference. School of Petrochemical Engineering, Lanzhou University of Technology; State Key Laboratory of Advanced Equipment Tribology, Department of Mechanical Engineering, Tsinghua University; 2024:6. DOI:10.26914/c. cnkihy. 2024. 026205.

[4] Shuai Mengxiao, Xi Wenjie, Zeng Guanglei.Fluid-structure interaction analysis of dry gas seal in tree-like trough[J]. Mechatronics Information, 2024, (16):41-46.) DOI: 10. 19514/ j. cnki.cn32-1628/tm.2024.16.012.

[5] WANG Hujun, XIE Zhengcan, ZHAO Xiuyuan, et al. Effect of wettability gradient on tribological behavior of biomimetic texture surface[J].Journal of Tribology, 2024, 44(03):300-311.

[6] WANG Yanhong. Research on the design and performance of liquid film sealing groove based on bat wing wings[D]. China University of Petroleum(East China), 2019.

[7] ZHAO Hongyan, ZHANG Pengfei, MA Yun, et al. Experimental and theoretical analysis of flow field display of bee flapping wings[J].Science China:Technological Sciences, 2014, 44(11):1211-1221.

[8] Xi Wenjie, Shuai Mengxiao, Zeng Guanglei. et al. Research on dry gas sealing performance of bionic bee wing groove [J]. Hydraulics, Pneumatics and Seal, 2025, 45(05):75-82.

[9] Zhu Weibing, Zhou Shengren, Wang Heshun. Journal of Xihua University(Natural Science Edition), 2010, 29(06):1-3+21.

[10] Lebeck A O. Principles and Design of Mechanical Seals [M]. New York: Wiley, 1992.

[11] Wu Tianhua, Wang Xiaomo,Xu Guoliang.Engineering heat transfer (2nd edition)[M].Wuhan:Huazhong University of Science and Technology Press, 2018.

[12] Mechanical Science; Study Data from H.S. Wang et al Provide New Insights into Mechanical Science (Research on the cone angle and clearance of main pump seal)[J].Journal of Technology & Science,2015.

[13] Gu Guangxi, Song Yuansen, Bai Shaoxian. Effect of surface waviness on upstream pumping characteristics of liquid elliptical hole end seal[J]. Lubrication and Sealing, 2024, 49(01):149-154.

[14] Su Wentao, Hu Shihong, Wang Lei, et al. Performance analysis and optimization selection of dynamic pressure mechanical seals[J]. Journal of China University of Petroleum(Natural Science Edition), 2023, 47(06):138-145.